Article

The OCT RNFL Probability Map and Artifacts Resembling Glaucomatous Damage

Sol La Bruna[1], Anvit Rai[1,2], Grace Mao[1], Jennifer Kerr[1], Heer Amin[1,3], Zane Z. Zemborain[1,4], Ari Leshno[5,6], Emmanouil Tsamis[1], Carlos Gustavo De Moraes[5], and Donald C. Hood[1,5]

[1] Department of Psychology, Columbia University, New York, NY, USA

[2] Albert Einstein College of Medicine, New York, NY, USA

[3] Vagelos College of Physicians and Surgeons, New York, NY, USA

[4] Department of Biomedical Engineering, Duke University, Durham, NC, USA

[5] Bernard and Shirlee Brown Glaucoma Research Laboratory, Department of Ophthalmology, Columbia University Irving Medical Center, New York, NY, USA

[6] Sackler Faculty of Medicine, Tel Aviv University, Tel Aviv, Israel

Correspondence: Donald C. Hood, Department of Psychology, Columbia University, 1190 Amsterdam Avenue, 5501, New York, NY 10027, USA. e-mail: dch3@columbia.edu

Purpose: The purpose of this study was to improve the diagnostic ability of the optical coherence tomography (OCT) retinal nerve fiber layer (RNFL) probability (p-) map by understanding the frequency and pattern of artifacts seen on the p-maps of healthy control (HC) eyes resembling glaucomatous damage.

Methods: RNFL p-maps were generated from wide-field OCT cube scans of 2 groups of HC eyes, 200 from a commercial normative group (HC-norm) and 54 from a prospective study group, as well as from 62 patient eyes, which included 32 with early glaucoma (EG). These 32 EG eyes had 24-2 mean deviation (MD) better than −6 dB and perimetric glaucoma as defined by 24-2 and 10-2 criteria. For the HC groups, "glaucoma-like" arcuates were defined as any red region near the temporal half of the disc.

Results: Seven percent of the 200 HC-norm and 11% of the 54 HC RNFL p-maps satisfied the definition of "glaucoma-like," as did all the patients' p-maps. The HC p-maps showed two general patterns of abnormal regions, "arcuate" and "temporal quadrant," and these patterns resembled those seen on some of the RNFL p-maps of the EG eyes. A "vertical midline" rule, which required the abnormal region to cross the vertical midline through the fovea, had a specificity of >99%, and a sensitivity of 75% for EG and 93% for moderate to advanced eyes.

Conclusions: Glaucoma-like artifacts on RNFL p-maps are relatively common and can masquerade as arcuate and/or widespread/temporal damage.

Translational Relevance: A vertical midline rule had excellent specificity. However, other OCT information is necessary to obtain high sensitivity, especially in eyes with early glaucoma.

Introduction

Optical coherence tomography (OCT) has become an invaluable tool in the diagnosis of glaucoma.[1–14] As retinal nerve fiber layer (RNFL) thinning is a key component of glaucoma, imaging techniques like OCT have allowed for the visualization and quantification of RNFL changes. Commercially available summary statistics of RNFL thickness are frequently used by clinicians to inform diagnostic decisions.[7,15–18] However, there are shortcomings to relying on these summary statistics.[10,19–26]

OCT imaging has allowed for the creation of three-dimensional RNFL thickness maps. From these thickness maps, commercial software generates RNFL probability (p-) maps by comparing a patient's local RNFL thickness values to those of an age-similar

healthy control (HC) group. The p-maps have shown clinical utility in the diagnosis of glaucoma.[6,13,27–36] Recently, these maps have been incorporated into a scheme to define and teach how to use OCT to detect damage based solely upon an OCT report.[37,38] Additionally, recent work in artificial intelligence (AI) suggests that the RNFL p-map is more useful than RNFL thickness maps, or than ganglion cell layer thickness or p-maps for differentiating healthy eyes from those with glaucoma.[39–41]

Although RNFL p-maps appear to be clinically useful, they are not immune to artifacts that can resemble damage due to glaucoma. For instance, it has been documented that confusion can arise due to arcuate artifacts on RNFL p-maps; these artifacts are examples of so-called "red disease,"[42] and are due to normal variations in the location of the major temporal blood vessels,[10,23,43] and the associated major RNFL bundles.[20,44] Unlike artifacts due to scanning or alignment errors, these arcuate artifacts are often confused with "real" arcuate defects caused by glaucomatous damage. Whereas the existence of these glaucoma-like artifacts is generally accepted,[10,42,43] less is known about their frequency. In addition, it is possible that there are other causes for patterns of seemingly abnormal regions on the RNFL p-maps that can also be confused with glaucomatous damage.

For the RNFL p-map to have high specificity, it is important to understand the nature and frequency of artifacts that can be confused with changes due to glaucoma. In this study, we seek to improve the use of the RNFL p-map by comparing artifacts seen on the RNFL p-maps of HC eyes with patterns of glaucomatous damage seen on RNFL p-maps of eyes with glaucoma of ranging severity. In particular, we address three questions: (1) what is the frequency of artifacts on HC RNFL p-maps that might be confused with abnormal patterns seen on the p-maps of patients? (2) what do these patterns look like? Finally, (3) we ask if a simple rule can help to distinguish between the patterns seen on HC artifacts and glaucomatous damage.

Methods

Study procedures followed the tenets of the Declaration of Helsinki and Health Insurance Portability and Accountability Act and were approved by the Institutional Review Board of Columbia University. Written informed consent was obtained from all participants.

Participants

The OCT data came from two sources. First, there were 145 eligible eyes from an observational, prospective, case-control study, the Macular Damage in Early Glaucoma and Progression Study (MAPS; PI: C Gustavo De Moraes; ClinicalTrials.gov Identifier: NCT02547740). All 145 eyes had at least 2 baseline OCT scans and 24-2 and 10-2 visual field (VF) within 13 days and had best-corrected visual acuity of 20/40 or better and refractive error between −6.00 and +6.00 diopters (D; spherical equivalent), the typical inclusion criterion for commercial normative groups. These 145 eyes included 54 HC eyes, 61 eyes with early glaucoma or suspected glaucoma (S/EG) with 24-2 VF mean deviation (MD) better than −6 dB from MAPS, as well as contralateral eyes of MAPS that included 12 eyes with moderate glaucoma (MG, 24-2 VF MD >-6 dB and <-12 dB), and 18 eyes with advanced glaucoma (AG; 24-2 VF MD >-12 dB). Four eyes were excluded from an initial group of 149 eyes as they had epiretinal membranes that affected OCT imaging.

All HCs had intraocular pressure (IOP) within statistically normal limits and normal fundus examination. These eyes had multiple 24-2 and 10-2 VFs, as well as OCT tests. Although the inclusion of these eyes was strictly based upon IOP and fundus examination, the OCT and VF tests were confirmatory. All patient eyes had a glaucoma, or glaucoma suspect, diagnosis based upon the referring glaucoma specialist's interpretation of functional (24-2 and 10-2 VFs) and structural (fundus photographs and OCT) information, as well as IOP and clinical history. All eyes had 24-2 and 10-2 VF tests with SITA-Standard protocol (Carl Zeiss Meditec, Inc., Dublin, CA) and OCT scans as described below.

To reduce the number of suspect eyes in the analysis and to form a group of eyes likely to have glaucoma based upon strictly functional information, we applied a modified Ocular Hypertension Treatment Study (OHTS) criteria to the 61 S/EG eyes. An eye was classified as EG_{VF} if three consecutive VFs were reliable VFs and met the criteria below. A reliable field was defined as one with false-positive (FP) errors and false-negative (FN) errors less than 15%, and with fixation losses less than 33%. Note that 33% is used as the limit for fixation losses for OHTS, in contrast to the HFA's default value of 20%. According to the OHTS protocol, an abnormal 24-2 VF is defined as having a glaucoma hemifield test (GHT) outside of normal limits and/or a pattern standard deviation (PSD) with $P < 0.05$ with the abnormality in the same hemifield across the 3 tests.[45,46] The OHTS protocol does not include the 10-2 VF. However, several recent
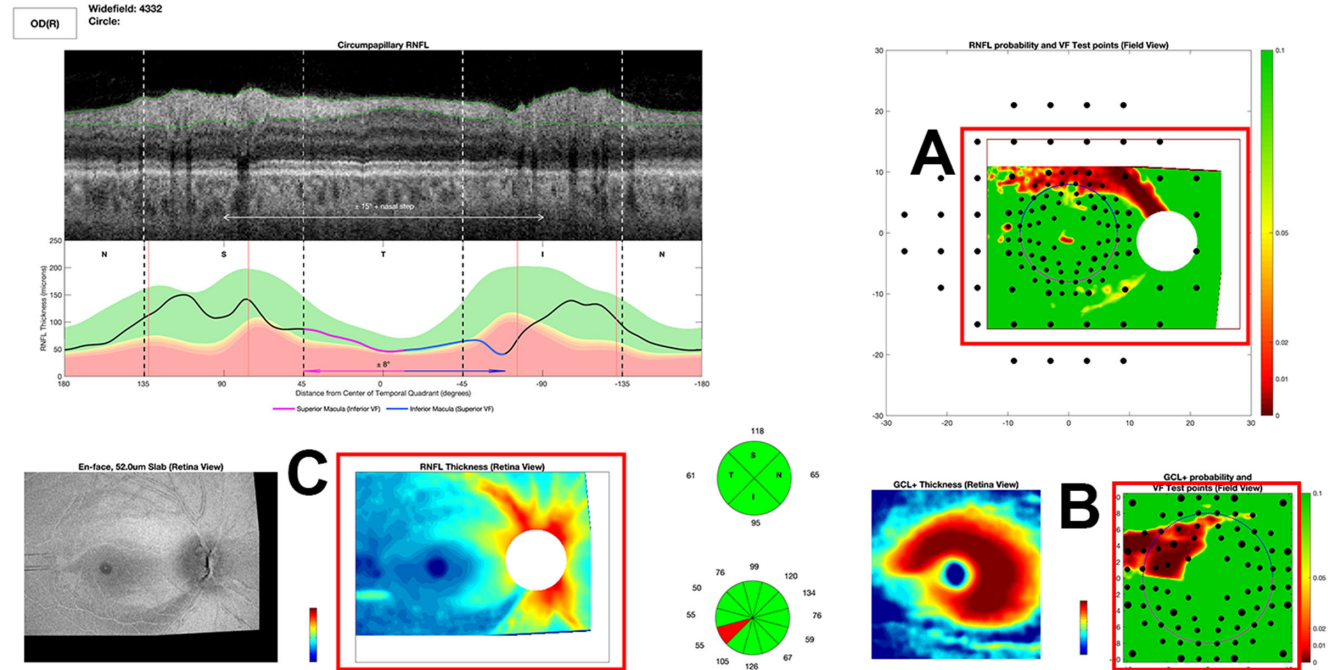
Figure 1. A research version of the commercially available Hood Report based upon a wide-field swept-source OCT volume scan. (**A**) The retinal nerve fiber layer probability map. (**B**) The ganglion cell plus inner plexiform layer probability map. Note that the probability maps are shown in field view so that the top of each corresponds to the upper visual field/inferior retina. (**C**) The RNFL thickness map, in retina view. See references for more details.[10,33]

publications have shown that eyes classified as normal by the OHTS criteria can have clear macular damage on the 10-2 VF.[47–50] Therefore, we applied a similar classification scheme for the 10-2, in which an abnormal 10-2 VF is defined as having an MD with $P \leq 0.05$ and/or a PSD with $P \leq 0.05$ with the abnormality in the same hemifield across the three tests. Of the 61 eyes, 32 had 3 consecutive abnormal 24-2 VFs or 3 consecutive abnormal 10-2 VFs (EG$_{VF}$).

An additional 200 healthy eyes (HC-norm) were included from a commercial normative reference group (data provided by Topcon Inc., Tokyo, Japan). These were the first 200, after excluding 2 eyes that had OCT reports consistent with optic neuropathy. In addition to arcuate defects seen on the p-maps, the en-face map, as in the lower left panel of Figure 1, showed a clear arcuate defect. Given the prevalence of glaucoma in the general populations,[51,52] and the fact that the 24-2 VF can miss this type of glaucomatous damage,[47,48] it is not surprising to find that 2 eyes, 1% among the 200 eyes, might have glaucoma. Because our purpose here was to understand "true" arcuates, these two eyes were excluded.

Optical Coherence Tomography

Wide-field (9×12 mm) swept-source OCT volume scans (Topcon, Inc.) were obtained for each eye, consisting of 256 B-scans, each with 512 A-scans. For the 145 MAPS eyes, in all but 1 case, the scan came from the first baseline visit. In that one case, the first baseline image suffered from poor focusing, so the second visit was used instead. In most cases, there was more than one scan available on the first baseline visit, so we used the same scan as the Sun et al. study.[53] In that study, every report and scan underwent quality assessment by two OCT experts/readers to identify the scan with the best quality from each study visit. Scans with incorrect centering, significant eye motion, or blink artifacts that would result in loss of measurements from the disc or macula were excluded. It is important to note that the exclusion criteria did not either directly or indirectly include artifacts that could be confused with glaucoma-like damage, which are the focus of the present study.

For the 200 HC-norm eyes, there was only one scan available per eye.

From the widefield scans, thickness values of the RNFL were extracted. A 6×6 mm region of the widefield scan, which was centered on the fovea, was used to obtain the thickness values of the retinal ganglion cell plus inner plexiform layer (GCL+) of the macular region. Using the reference database from the OCT device manufacturers, we generated age-corrected p-maps, used in an established OCT wide-field report that is commercially available outside of the United States. Figure 1 provides an example of the OCT wide-field report. This study focused predominantly on the two framed p-maps: the RNFL p-map (A) and the GCL+ p-map (B) in Figure 1. Both p-maps are in field view so that the upper region corresponds to the superior VF/the inferior retina. The symbols seen on the p-maps in all figures indicate the location of the 24-2 (larger symbols) and 10-2 (smaller symbols) VF test points.

Identifying Glaucoma-Like Artifacts on HC RNFL p-Maps

To identify glaucoma-like abnormal patterns on the RNFL p-maps, we assumed that a red region near the temporal half of the disc is a necessary condition to classify an RNFL p-map as "abnormal." This necessary condition for glaucoma was based upon the observation documented below that all the patients with glaucoma met this condition. Using this definition, 3 authors (S.L.B., A.R., and D.C.H.) separately scrutinized the 54 HC p-maps and the 200 HC-norm p-maps. In instances of disagreement, there was adjudication, and a consensus was reached. In the case of the 54 HC from MAPS, all the p-maps are presented below so the readers can make their own judgment (Fig. 2A).

Metric Analyses

To compare the HC eyes with glaucoma-like artifacts to the most commonly used summary statistic of RNFL thickness, for each eye, we calculated the global (average) circumpapillary (cpRNFL) thickness (G_{cpRNFL}) using the wide-field OCT scan and derived B-scan image for the 3.4-mm diameter circle, as previously described.[50]

Results

Based upon the inclusion criteria discussed above, the analysis of RNFL p-maps included 54 HC, 32 EG_{VF}, 12 MG, 18 AG, and 200 HC-norm eyes. Figure 2 shows the RNFL p-maps for the first 4 of these groups.

Identifying Artifacts in HCs that may be Confused With Glaucomatous Damage

The RNFL p-maps in Figure 2 are ordered based upon the G_{cpRNFL}. For example, for the 54 HC eyes (see Fig. 2A), the thinnest G_{cpRNFL} (#1) is in the lower left and the thickest (#54) is in the upper right. We chose G_{cpRNFL} as it is a common OCT measure of severity of damage.[16,35,54–62]

Notice that all the 62 AG/MG/EG_{vf} eyes in panels B to D of Figure 2 have a red region near the temporal side of the disc, consistent with our working hypothesis, which assumed that a red region near the temporal half of the disc is a necessary condition to classify an RNFL p-map as abnormal. Although this appears to be a necessary condition, it is not sufficient as 6 (11%) of the RNFL p-maps of the 54 HCs met this condition. These 6 p-maps have a red border in Figure 2A and enlarged versions of these 6 p-maps are shown in Figure 3A. These are the HC RNFL p-maps that the clinician might confuse with those from eyes with glaucomatous damage.

To enlarge our sample of HCs with artifacts, we examined 200 RNFL p-maps from a commercial database mentioned in the Methods. Of these 200, 14 (7%) had artifacts defined as a red region on the temporal half of the disc. The RNFL p-maps for these 14 are shown in Figure 3B.

Classification of RNFL p-Map Artifacts in HC

The artifacts identified in the HC RNFL p-maps appeared to fall into three groups (as indicated in Figs. 3A,B): (1) "arcuate": an arcuate-shaped artifact that could be mistaken for arcuate damage commonly seen in glaucoma; (2) "temporal quadrant (Q)": artifacts that include the temporal Q of the disc and the maculo-papillary region of the p-map; they can be mistaken for maculo-papillary and/or diffuse glaucomatous damage; and (3) "both": artifacts that appeared to be a combination of the two. The Table shows the number of cases for each type of artifact for the HC and HC-norm groups.

A "Vertical Midline" Rule for Identifying HC Artifacts

To minimize FP results and obtain high sensitivity, we assumed as a working hypothesis that the abnormal region on the RNFL p-map must cross the midline (the black vertical lines through the center of the fovea in Figs. 3A,B). The anatomic basis for this "vertical midline rule" has to do with the observation that
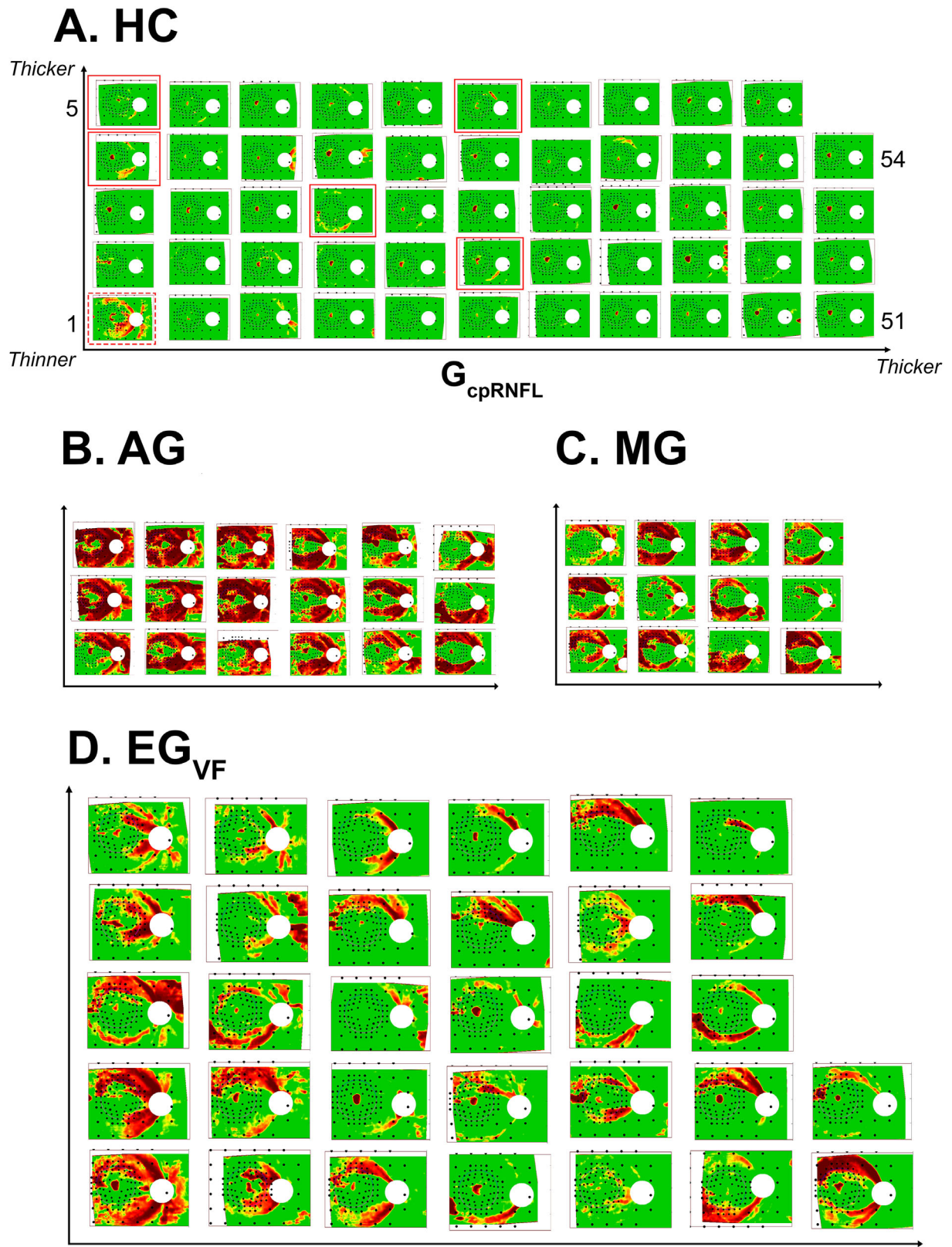
Figure 2. The retinal nerve fiber layer (RNFL) probability (p-) maps ordered by global circumpapillary RNFL thickness (G_{cpRNFL}) for each of the groups. For each panel, the thinnest G_{cpRNFL} is in the lower left and the thickest is in the upper right. (**A**) The RNFL p-maps ordered by G_{cpRNFL} for the 54 healthy controls (HCs). (**B**) Same as panel **A**, but for the 18 advanced glaucoma (AG) eyes. (**C**) Same as panel **A**, but for the 12 moderate glaucoma (MG) eyes. (**D**) Same as panel **A**, but for the 32 early glaucoma eyes (EG_{VF}) that meet the modified Ocular Hypertension Treatment Study (OHTS) criteria.
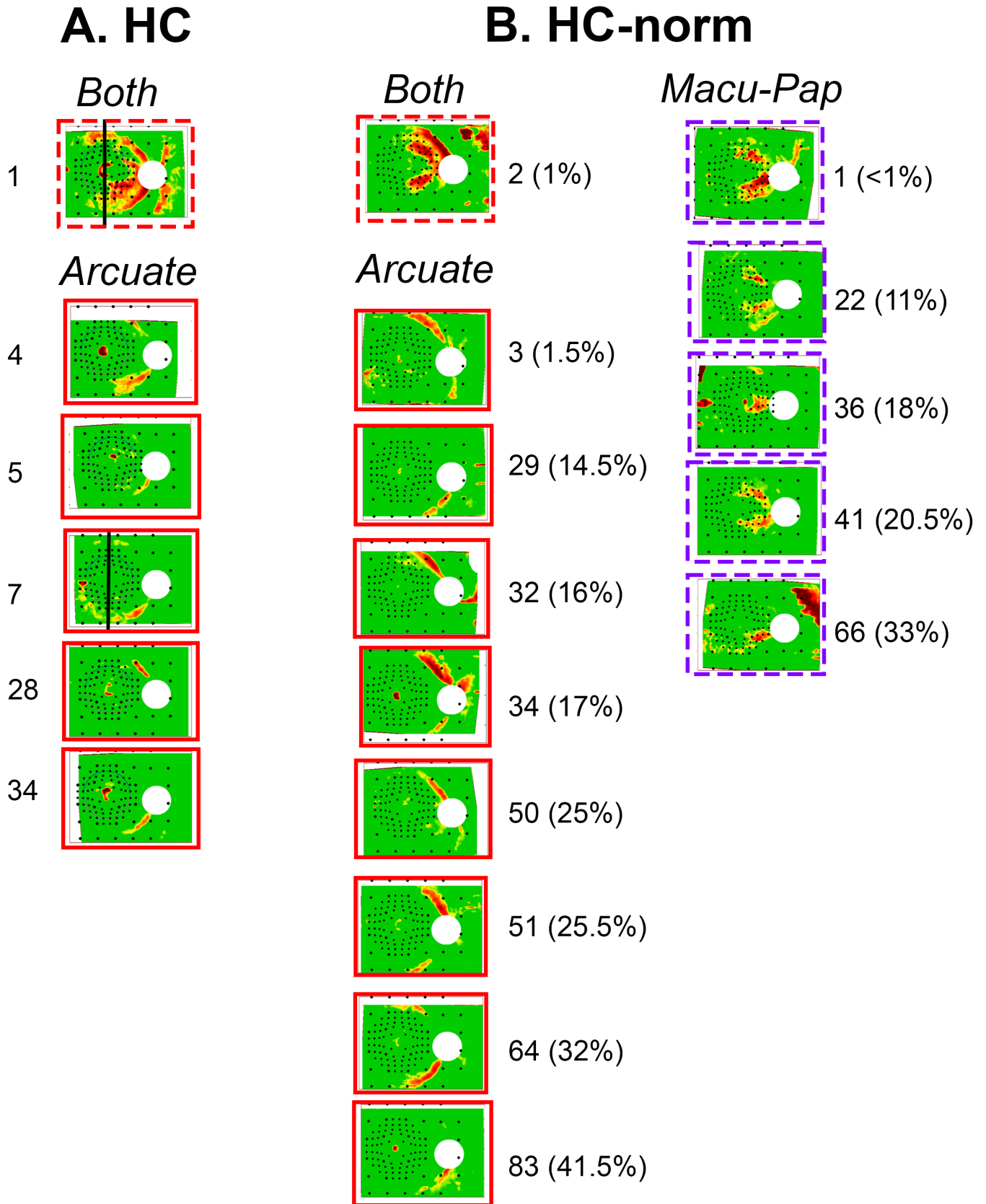
A. HC

B. HC-norm

Both

Both

Macu-Pap

1

2 (1%)

1 (<1%)

Arcuate

Arcuate

22 (11%)

4

3 (1.5%)

36 (18%)

5

29 (14.5%)

41 (20.5%)

7

32 (16%)

66 (33%)

28

34 (17%)

34

50 (25%)

51 (25.5%)

64 (32%)

83 (41.5%)

Figure 3. The RNFL p-maps of HC eyes that could be mistaken for glaucoma. (**A**) The 6 RNFL p-maps of the 54 HC with an "arcuate" artifact (*solid red border*) or with both a "temporal quadrant (Q)" and "arcuate" artifact (*dashed red border*). The numbers next to the RNFL p-maps

→

←

describe the position in the distribution as the *n*th thinnest (i.e. for the RNFL p-map in the top left, it is the thinnest [first], whereas the one below is the fourth thinnest). The *black line* on two of the RNFL p-maps denote the vertical midline through the fovea. (**B**) The 14 RNFL p-maps of the 200 healthy controls from a commercial normative database (HC-norm) that have an "arcuate" artifact (*red border*), a "temporal (Q)" artifact (*dashed purple border*), or both (*dashed red border*). The numbers next to the RNFL p-maps describe the position in the distribution as the *n*th thinnest, as well as its percentile position in the distribution. For example, the first p-map in the top left column is the second thinnest and is in the first percentile.

Table. Total Number of Glaucoma-Like Artifacts in HCs

Group	Arcuate	Temporal Q	Both
HC-norm ($n = 200$)	8	5	1
HC ($n = 54$)	5	0	1
Total ($n = 254$)	13 (5%)	5 (2%)	2 (<1%)

HC, healthy control; HC-norm, healthy control commercial normative group.

arcuate artifacts seen on RNFL p-maps of HCs are associated with displacement of the major temporal arcuate bundles of the RNFL.[10,23] Notice in Figure 3A and B that the abnormal red/yellow region crosses the midline (black vertical line in Fig. 3A) in only 2 of the 15 RNFL p-maps with "arcuate" artifacts. Although it is likely that the "temporal Q" artifacts are due to more than one deviation from normal anatomy, they too do not cross the midline in the RNFL p-map of HCs. In fact, none of the 5 "temporal Q" artifacts in Figure 3B cross the midline.

The Sensitivity of the Vertical Midline Rule

All of the AG, and all but two of the MG, RNFL p-maps showed abnormal arcuate regions that cross the midline, for a sensitivity of 93% for the combined MG/AG eyes. On the other hand, the sensitivity for the EG_{VF} group was only 75%, as 8 of the 32 failed the midline test. Thus, based upon the vertical midline rule, there were 2 FP results (99.2% of 254, HC plus HC-norm) and 10 FN results (84% of the 62 AG/MG/EG_{vf}). Figure 4A shows the RNFL p-maps for these FP and FN results. Notice that these p-maps overlap in appearance.

Relation of RNFL p-Map Artifacts to cpRNFL Thickness

As G_{cpRNFL} thickness is a commonly used single OCT measure of RNFL damage, we asked if it was a good predictor of the artifacts seen in RNFL p-maps. Figure 5 shows a histogram of the distribution of G_{cpRNFL} thicknesses for the HC (A), HC-norm (B), and EG_{VF} (C) groups. The vertical dotted line within each panel indicates the average G_{cpRNFL} thickness for

that group, and the red vertical line represents the 5% lower percentile calculated from the HC-norm. For the HC groups in panels A and B of Figure 5, eyes falling to the left of this vertical red line are FP results.

There are two aspects of note in panels A and B of Figure 5. First, the RNFL p-maps of some of the G_{cpRNFL} FP results are unambiguously normal. For example, the RNFL p-maps within the black boxes have little or no red region, or a red region that is clearly not due to glaucoma (e.g. small red regions near fixation or scanning artifacts, orange arrows). Second, some of the HC RNFL p-maps with arcuate artifacts, which the clinician might mistake for glaucomatous damage, have G_{cpRNFL} thicknesses well above the 5th percentile of the HC-norm, as indicated by the insets with red borders in Figure 5A and B and the percentiles in parentheses in Figure 3B.

Discussion

As clinicians increasingly rely on OCT RNFL p-maps, it is important to understand the artifacts in RNFL p-maps of HCs. Whereas previous work on artifacts have generally focused on scanning artifacts due to eye movements, segmentation errors, and centering,[22,24,25,63–69] we focused on glaucoma-like artifacts. As detailed below, we addressed three questions. First, what was the frequency of artifacts on HC RNFL p-maps that could be confused with abnormal patterns seen on the p-maps of patients? Second, what do the p-maps of HCs that could be mistaken for glaucoma look like? Finally, we asked if a simple rule, the vertical midline rule, could help to distinguish between the HC artifacts and glaucomatous damage.

The Frequency and Patterns of Glaucoma-Like Artifacts

About 11% of the HC p-maps had artifacts resembling the general patterns seen in patients with glaucoma. Further, we found that these glaucoma-like artifacts take on two general forms: (1) "arcuate": an arcuate-shaped artifact that could be mistaken for arcuate damage commonly seen in glaucoma; and (2)
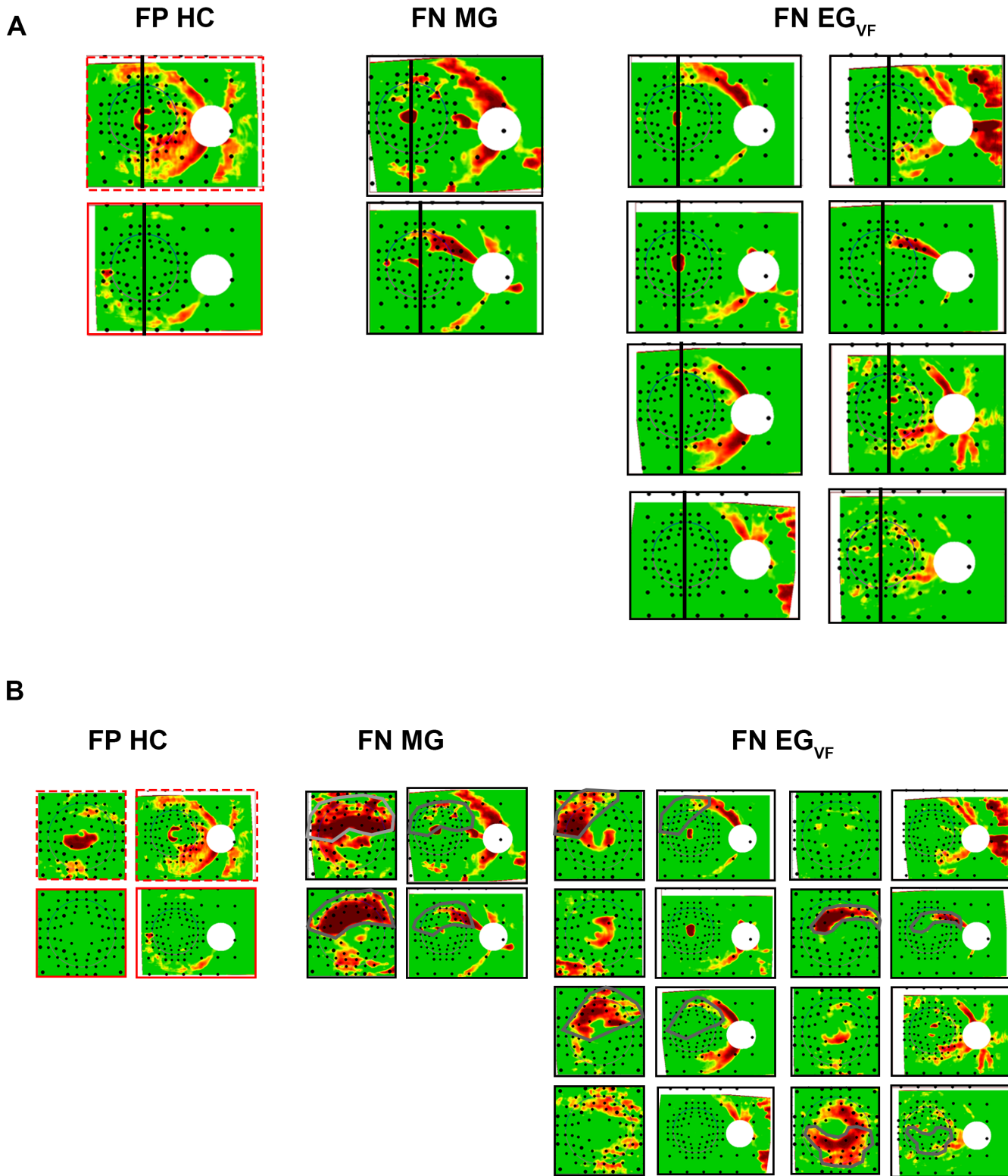
Figure 4. (**A**) The RNFL p-maps of FP results and FN results based on the midline rule. RNFL p-maps that have an "arcuate" artifact (red border), or both an "arcuate" and "temporal Q" artifact, are outlined (*dashed red border*), whereas patient eyes are outlined with *black borders*. The *black line* on each RNFL p-map demarcates the vertical midline through the fovea. (**B**) The same, but the RNFL p-maps are accompanied by their corresponding ganglion cell plus inner plexiform layer (GCL+) p-map. Those patient eyes with topographically correspondent damage on the RNFL and GCL+ p-map have arcuate lines demonstrating the regions of damage.
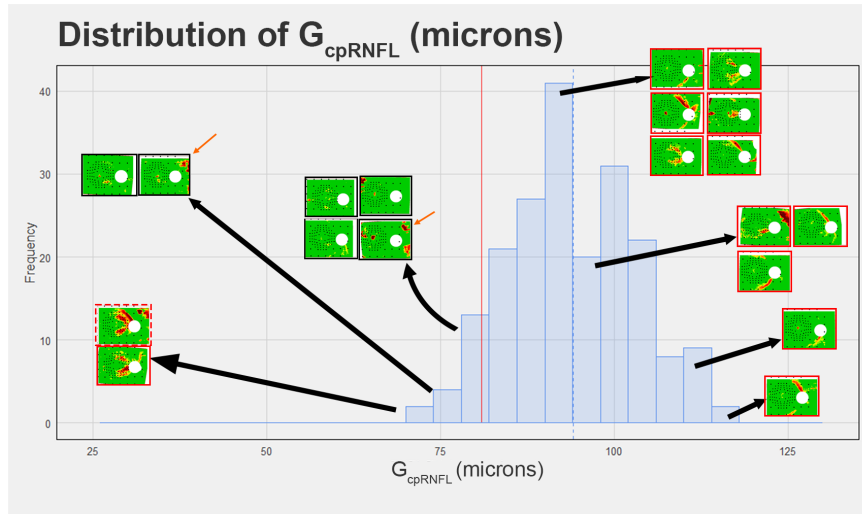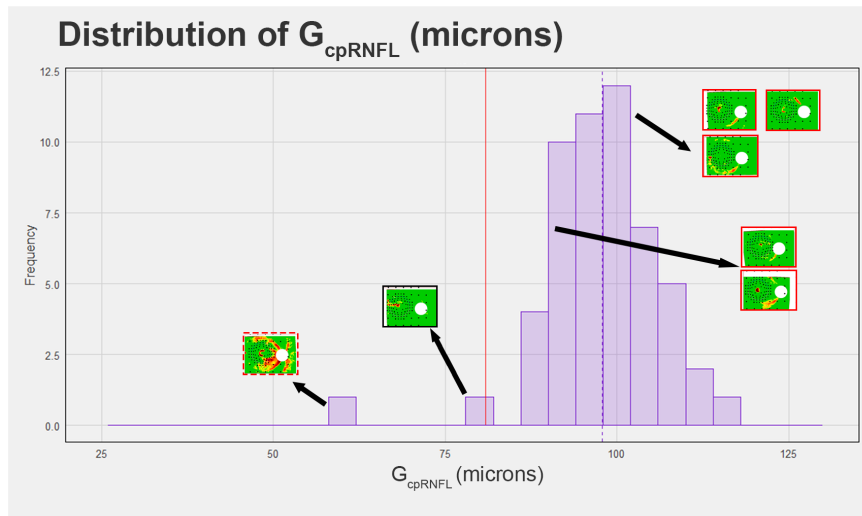
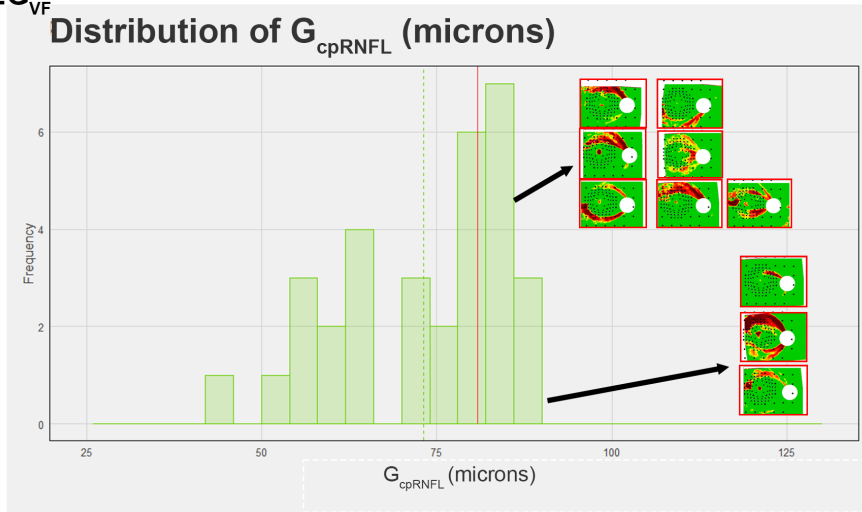**Figure 5.** Histogram distributions of G_{cpRNFL} thickness for the (**A**) HC-norm, (**B**) HC, and (**C**) EG_{VF}. The *red line* provides the bottom fifth percentile threshold calculated from the HC-norm. The *dashed line* on each panel provides the average G_{cpRNFL} for each group. The position

→

←
of the individual p-maps along the distributions are depicted by *black arrows*. The *red*, *solid borders* and *dashed red borders* surrounding p-maps provide examples of eyes that, in **A** and **B**, could be mistaken as glaucomatous (the *solid red border* indicates "arcuate" artifacts and the *dashed red borders* indicate both "temporal Q" and "arcuate" artifacts), and in (**C**), that have glaucoma. The RNFL p-maps with *black borders* in **A** and **B** are eyes that are unambiguously normal. The *orange arrows* in **A** point to instances in which there are scanning artifacts. In **A** and **B**, eyes on the left of the *red line* are false positive results (FPs), whereas eyes on the right of the *red line* in **C** are false negative results (FNs).

"temporal Q": artifacts associated with the temporal quadrant of the disc and that could be mistaken for maculo-papillary damage and/or diffuse damage. A third, and less frequent, group includes eyes with both "arcuate" and "temporal Q" artifacts.

"Arcuate" artifacts were the most common type of artifact, and previous work suggests that these artifacts may be caused by anatomic variations in the location of blood vessels and the associated RNF bundles.[10,20,23,43,44] "Temporal Q" artifacts were less common and proved more difficult to distinguish from HCs, as discussed next.

The Vertical Midline Rule

We hypothesized that "arcuate" artifacts should not cross the midline, defined as a vertical line through the fovea (see Fig. 2A, Fig. 4A). This vertical midline rule is based upon the observation that arcuate artifacts seen on RNFL p-maps of HCs are associated with displacement of the major temporal arcuate bundles of RNFL, whereas true glaucomatous damage follows arcuates that cross the midline outside the maculo-papillary bundle. In any case, the rule, as expected, had excellent specificity. Only 2 of the 254 HC eyes crossed the midline. That is, the specificity was about 99%.

Beyond the Vertical Midline Rule

On the other hand, the vertical midline rule missed glaucomatous damage, especially in EG_{VF} eyes. Out of the 62 AG/MG/EG_{vf} eyes, there were 10 FN results (84% sensitivity) with 8 of these 10 being EG_{vf} eyes for a sensitivity of 75% for EG_{vf} eyes. It is possible that other aspects of the patterns seen on RNFL p-maps can be used to distinguish between HCs and EG_{vf} eyes. For example, a visual examination of the EG_{vf} p-map patterns in Figure 2D, which do not cross the vertical midline, suggests that they tend to have deeper, wider, and more extensive abnormal regions than the HC artifacts in Figure 3. However, there is an overlap in appearance that will make it difficult for a clinician to reliably use this information. It is possible, however, that an AI program based upon RNFL p-maps, such as that developed by Thakoor and colleagues,[40,70,71] may be able to use this information.

However, it is important to note that the vertical midline rule *only* uses the OCT RNFL p-map. Other information on the OCT report in Figure 1 can help to distinguish between eyes with early glaucoma and HCs.[37,38] As an illustration, in Figure 4B we show the GCL+ p-maps for the FP results and FN results in Figure 4A. For at least 6 of the 10 FN results, GCL+ p-maps clearly confirm that the arcuate seen on the RNFL p-map is consistent with glaucoma. Note in these six eyes, the combined abnormal region on the GCL+ and RNFL p-maps does cross the midline (Fig. 4B). See figure caption for details.

Limitations

Our study has the following limitations. First, a similar analysis should be made for other OCT models and manufacturers. It is unlikely that the manufacturer or make of the OCT instrument per se will be a significant factor, as the major source of these artifacts is anatomic variation among the HC eyes. On the other hand, the frequency of the glaucoma-like defects will certainly be impacted by the composition of the control group, as well as the software used to produce the p-maps from thickness maps; both control group composition and methodology for producing p-maps vary across manufacturers.

Another limitation is the sample size of the glaucomatous eyes. A replication with a larger sample size of glaucomatous eyes of varying severities should be performed. Additionally, this study did not include eyes with high myopia, although it should be possible to analyze the p-maps in many eyes with high myopia.[72]

It might be argued that the use of the modified OHTS criteria to select EG eyes is a limitation. In fact, this may have resulted in the elimination of some EG eyes with even more subtle damage than seen in the EG_{vf}, although it is not clear how this would impact the conclusions here. In any case, we did not want to confuse the analysis with EG eyes that were in fact healthy. Further, we could argue that the use of functional inclusion criteria to examine structural data is a strength of the design.

Finally, our analysis did not take into consideration that these artifacts may be present in eyes with glaucoma as well. If, as we suspect, anatomic

variation is the source of these artifacts, then they should be present in approximately the same percentage in eyes with EG. For example, we should expect about 3 (10%) of the 32 EG$_{vf}$ eyes to be influenced. Although given the patterns we see in the HC p-maps in Figure 2, in most cases. the impact should be minor.

Conclusions

Glaucoma-like artifacts on RNFL probability maps are relatively common and can masquerade as arcuate and/or widespread and/or temporal damage. These artifacts are characterized by a failure for the abnormal region to cross the vertical midline. Although the vertical midline rule had excellent specificity, other OCT information is necessary to avoid FN results and to obtain high sensitivity, especially in eyes with early glaucoma.

Acknowledgments

Disclosure: **S.L. Bruna,** None; **A. Rai,** None; **G. Mao,** None; **J. Kerr,** None; **H. Amin,** None; **Z.Z. Zemborain,** None; **A. Leshno,** None; **E. Tsamis,** None; **C.G. De Moraes,** Carl Zeiss Meditec, Inc. (R), Topcon, Inc. (R), Heidelberg Engineering (R), Novartis, Inc. (C), Galimedix, Inc. (C), Lin Biosciences, Inc. (C), Reichert, Inc. (C); **D.C. Hood,** Topcon, Inc. (F, C), Heidelberg Engineering (F, C), Novartis, Inc. (C)

References

1. Huang D, Swanson EA, Lin CP, et al. Optical Coherence Tomography. *Science*. 1991;254(5035):1178–1181.
2. Jaffe GJ, Caprioli J. Optical coherence tomography to detect and manage retinal disease and glaucoma. *Am J Ophthalmol*. 2004;137(1):156–169.
3. Sharma P, Sample PA, Zangwill LM, Schuman JS. Diagnostic Tools for Glaucoma Detection and Management. *Surv Ophthalmol*. 2008;53(6, Supplement):S17–S32.
4. Sung KR, Kim JS, Wollstein G, Folio L, Kook MS, Schuman JS. Imaging of the retinal nerve fibre layer with spectral domain optical coherence tomography for glaucoma diagnosis. *Br J Ophthalmol*. 2011;95(7):909–914.
5. Stein JD, Talwar N, LaVerne AM, Nan B, Lichter PR. Trends in Use of Ancillary Glaucoma Tests for Patients with Open-Angle Glaucoma from 2001 to 2009. *Ophthalmology*. 2012;119(4):748–758.
6. Hood DC, Raza AS. On improving the use of OCT imaging for detecting glaucomatous damage. *Br J Ophthalmol*. 2014;98(Suppl 2):ii1–ii9.
7. Bussel II, Wollstein G, Schuman JS. OCT for glaucoma diagnosis, screening and detection of glaucoma progression. *Br J Ophthalmol*. 2014;98(Suppl 2):ii15–ii19.
8. Gracitelli CPB, Abe RY, Medeiros FA. Spectral-Domain Optical Coherence Tomography for Glaucoma Diagnosis. *Open Ophthalmol J*. 2015;9:68–77.
9. Mwanza JC, Budenz DL. Optical coherence tomography platforms and parameters for glaucoma diagnosis and progression. *Curr Opin Ophthalmol*. 2016;27(2):102–110.
10. Hood DC. Improving our understanding, and detection, of glaucomatous damage: An approach based upon optical coherence tomography (OCT). *Prog Retin Eye Res*. 2017;57:46–75.
11. Hood DC, De Moraes CG. Four Questions for Every Clinician Diagnosing and Monitoring Glaucoma. *J Glaucoma*. 2018;27(8):657–664.
12. Hood DC, De Moraes CG. Challenges to the Common Clinical Paradigm for Diagnosis of Glaucomatous Damage With OCT and Visual Fields. *Invest Ophthalmol Vis Sci*. 2018;59(2):788–791.
13. Chen TC, Hoguet A, Junk AK, et al. Spectral-Domain OCT: Helping the Clinician Diagnose Glaucoma: A Report by the American Academy of Ophthalmology. *Ophthalmology*. 2018;125(11):1817–1827.
14. Geevarghese A, Wollstein G, Ishikawa H, Schuman JS. Optical Coherence Tomography and Glaucoma. *Annu Rev Vis Sci*. 2021;7(1):693–726.
15. Vessani RM, Moritz R, Batis L, Zagui RB, Bernardoni S, Susanna R. Comparison of quantitative imaging devices and subjective optic nerve head assessment by general ophthalmologists to differentiate normal from glaucomatous eyes. *J Glaucoma*. 2009;18(3):253–261.

16. Sung KR, Kim DY, Park SB, Kook MS. Comparison of retinal nerve fiber layer thickness measured by Cirrus HD and Stratus optical coherence tomography. *Ophthalmology*. 2009;116(7):1264–1270, 1270.e1.

17. Kansal V, Armstrong JJ, Pintwala R, Hutnik C. Optical coherence tomography for glaucoma diagnosis: An evidence based meta-analysis. *PLoS One*. 2018;13(1):e0190621.

18. Ha A, Park KH. Optical Coherence Tomography for the Diagnosis and Monitoring of Glaucoma. *Asia-Pac J Ophthalmol*. 2019;8(2):135–145.

19. Kim NR, Lim H, Kim JH, Rho SS, Seong GJ, Kim CY. Factors Associated with False Positives in Retinal Nerve Fiber Layer Color Codes from Spectral-Domain Optical Coherence Tomography. *Ophthalmology*. 2011;118(9):1774–1781.

20. Hood DC, Raza AS, de Moraes CGV, Liebmann JM, Ritch R. Glaucomatous damage of the macula. *Prog Retin Eye Res*. 2013;32:1–21.

21. Kim KE, Jeoung JW, Park KH, Kim DM, Kim SH. Diagnostic classification of macular ganglion cell and retinal nerve fiber layer analysis: differentiation of false-positives from glaucoma. *Ophthalmology*. 2015;122(3):502–510.

22. Lee SY, Kwon HJ, Bae HW, et al. Frequency, Type and Cause of Artifacts in Swept-Source and Cirrus HD Optical Coherence Tomography in Cases of Glaucoma and Suspected Glaucoma. *Curr Eye Res*. 2016;41(7):957–964.

23. Chen JJ, Kardon RH. Avoiding Clinical Misinterpretation and Artifacts of Optical Coherence Tomography Analysis of the Optic Nerve, Retinal Nerve Fiber Layer, and Ganglion Cell Layer. *J Neuroophthalmol*. 2016;36(4):417–438.

24. Mansberger SL, Menda SA, Fortune BA, Gardiner SK, Demirel S. Automated Segmentation Errors When Using Optical Coherence Tomography to Measure Retinal Nerve Fiber Layer Thickness in Glaucoma. *Am J Ophthalmol*. 2017;174:1–8.

25. Nagarkatti-Gude N, Gardiner SK, Fortune B, Demirel S, Mansberger SL. Optical Coherence Tomography Segmentation Errors of the Retinal Nerve Fiber Layer Persist Over Time. *J Glaucoma*. 2019;28(5):368–374.

26. Hood DC, Tsamis E, Bommakanti NK, et al. Structure-Function Agreement Is Better Than Commonly Thought in Eyes With Early Glaucoma. *Invest Ophthalmol Vis Sci*. 2019;60(13):4241–4248.

27. Leung CKS, Lam S, Weinreb RN, et al. Retinal nerve fiber layer imaging with spectral-domain optical coherence tomography: analysis of the retinal nerve fiber layer map for glaucoma detection. *Ophthalmology*. 2010;117(9):1684–1691.

28. Leung CKS, Choi N, Weinreb RN, et al. Retinal nerve fiber layer imaging with spectral-domain optical coherence tomography: pattern of RNFL defects in glaucoma. *Ophthalmology*. 2010;117(12):2337–2344.

29. Kim NR, Lee ES, Seong GJ, Choi EH, Hong S, Kim CY. Spectral-Domain Optical Coherence Tomography for Detection of Localized Retinal Nerve Fiber Layer Defects in Patients With Open-Angle Glaucoma. *Arch Ophthalmol*. 2010;128(9):1121–1128.

30. Sakamoto A, Hangai M, Nukada M, et al. Three-Dimensional Imaging of the Macular Retinal Nerve Fiber Layer in Glaucoma with Spectral-Domain Optical Coherence Tomography. *Invest Ophthalmol Vis Sci*. 2010;51(10):5062–5070.

31. Ye C, To E, Weinreb RN, et al. Comparison of Retinal Nerve Fiber Layer Imaging by Spectral Domain Optical Coherence Tomography and Scanning Laser Ophthalmoscopy. *Ophthalmology*. 2011;118(11):2196–2202.

32. Shin JW, Uhm KB, Lee WJ, Kim YJ. Diagnostic ability of retinal nerve fiber layer maps to detect localized retinal nerve fiber layer defects. *Eye*. 2013;27(9):1022–1031.

33. Hood DC, Cuir ND, Blumberg DM, et al. A Single Wide-Field OCT Protocol Can Provide Compelling Information for the Diagnosis of Early Glaucoma. *Transl Vis Sci Technol*. 2016;5(6):4.

34. Lee WJ, Na KI, Kim YK, Jeoung JW, Park KH. Diagnostic Ability of Wide-field Retinal Nerve Fiber Layer Maps Using Swept-Source Optical Coherence Tomography for Detection of Preperimetric and Early Perimetric Glaucoma. *J Glaucoma*. 2017;26(6):577–585.

35. Lee WJ, Oh S, Kim YK, Jeoung JW, Park KH. Comparison of glaucoma-diagnostic ability between wide-field swept-source OCT retinal nerve fiber layer maps and spectral-domain OCT. *Eye*. 2018;32(9):1483–1492.

36. Kim H, Park HM, Jeong HC, et al. Wide-field optical coherence tomography deviation map for early glaucoma detection. *Br J Ophthalmol*. Published online July 21, 2021, https://doi.org/10.1136/bjophthalmol-2021-319509.

37. Liebmann JM, Hood DC, de Moraes CG, et al. Rationale and development of an OCT-based method for detection of glaucomatous optic neuropathy. *J Glaucoma*. Published online February 28, 2022, doi:10.1097/IJG.0000000000002005.

38. Hood DC, La Bruna S, Tsamis E, et al. Detecting glaucoma with only OCT: Implications for

the clinic, research, screening, and AI development. *Prog Retin Eye Res.* Published online February 22, 2022:101052, doi:10.1016/j.preteyeres.2022.101052.

39. Muhammad H, Fuchs TJ, De Cuir N, et al. Hybrid deep learning on single wide-field optical coherence tomography scans accurately classifies glaucoma suspects. *J Glaucoma.* 2017;26(12):1086–1094.

40. Thakoor KA, Li X, Tsamis E, Sajda P, Hood DC. Enhancing the Accuracy of Glaucoma Detection from OCT Probability Maps using Convolutional Neural Networks. In: *2019 41st Annual International Conference of the IEEE Engineering in Medicine and Biology Society (EMBC).* 2019:2036–2040.

41. Shin Y, Cho H, Jeong HC, Seong M, Choi JW, Lee WJ. Deep Learning-based Diagnosis of Glaucoma Using Wide-field Optical Coherence Tomography Images. *J Glaucoma.* 2021;30(9):803–812.

42. Chong GT, Lee RK. Glaucoma versus red disease: imaging and glaucoma diagnosis. *Curr Opin Ophthalmol.* 2012;23(2):79–88.

43. La Bruna S, Tsamis E, Zemborain ZZ, et al. A Topographic Comparison of OCT Minimum Rim Width (BMO-MRW) and Circumpapillary Retinal Nerve Fiber Layer (cRNFL) Thickness Measures in Eyes With or Suspected Glaucoma. *J Glaucoma.* 2020;29(8):671–680.

44. Chen JJ, Kardon RH, Longmuir RA. Diagnostic features of retinal nerve fiber layer rotation in skew deviation using optical coherence tomography. *J Neuro-Ophthalmol Off J North Am Neuro-Ophthalmol Soc.* 2014;34(4):389–392.

45. Keltner JL, Johnson CA, Quigg JM, Cello KE, Kass MA, MO Gordon. Confirmation of visual field abnormalities in the Ocular Hypertension Treatment Study. Ocular Hypertension Treatment Study Group. *Arch Ophthalmol Chic Ill 1960.* 2000;118(9):1187–1194.

46. Keltner JL, Johnson CA, Cello KE, et al. Classification of visual field abnormalities in the ocular hypertension treatment study. *Arch Ophthalmol Chic Ill 1960.* 2003;121(5):643–650.

47. Grillo LM, Wang DL, Ramachandran R, et al. The 24-2 Visual Field Test Misses Central Macular Damage Confirmed by the 10-2 Visual Field Test and Optical Coherence Tomography. *Transl Vis Sci Technol.* 2016;5(2):15.

48. De Moraes CG, Hood DC, Thenappan A, et al. 24-2 Visual Fields Miss Central Defects Shown on 10-2 Tests in Glaucoma Suspects, Ocular Hypertensives, and Early Glaucoma. *Ophthalmology.* 2017;124(10):1449–1456.

49. Tsamis E, Bommakanti NK, Sun A, Thakoor KA, Moraes CGD, Hood DC. An Automated Method for Assessing Topographical Structure–Function Agreement in Abnormal Glaucomatous Regions. *Transl Vis Sci Technol.* 2020;9(4):14.

50. Tsamis E, La Bruna S, Leshno A, De Moraes CG, Hood DC. Detection of Early Glaucomatous Damage: Performance of Summary Statistics from Optical Coherence Tomography and Perimetry. In press.

51. Rudnicka AR, Mt-Isa S, Owen CG, Cook DG, Ashby D. Variations in Primary Open-Angle Glaucoma Prevalence by Age, Gender, and Race: A Bayesian Meta-Analysis. *Invest Ophthalmol Vis Sci.* 2006;47(10):4254–4261.

52. Cook C, Foster P. Epidemiology of glaucoma: what's new? *Can J Ophthalmol.* 2012;47(3):223–226.

53. Sun A, Tsamis E, Eguia MD, et al. Global optical coherence tomography measures for detecting the progression of glaucoma have fundamental flaws. *Eye (Lond).* 2021;35(11):2973–2982.

54. Schuman JS, Hee MR, Puliafito CA, et al. Quantification of nerve fiber layer thickness in normal and glaucomatous eyes using optical coherence tomography. *Arch Ophthalmol Chic Ill 1960.* 1995;113(5):586–596.

55. Zangwill LM, Williams J, Berry CC, Knauer S, Weinreb RN. A comparison of optical coherence tomography and retinal nerve fiber layer photography for detection of nerve fiber layer damage in glaucoma. *Ophthalmology.* 2000;107(7):1309–1315.

56. Bowd C, Zangwill LM, Berry CC, et al. Detecting Early Glaucoma by Assessment of Retinal Nerve Fiber Layer Thickness and Visual Function. *Invest Ophthalmol Vis Sci.* 2001;42(9):1993–2003.

57. Kanamori A, Nakamura M, Escano MFT, Seya R, Maeda H, Negi A. Evaluation of the glaucomatous damage on retinal nerve fiber layer thickness measured by optical coherence tomography. *Am J Ophthalmol.* 2003;135(4):513–520.

58. Nouri-Mahdavi K, Hoffman D, Tannenbaum DP, Law SK, Caprioli J. Identifying early glaucoma with optical coherence tomography. *Am J Ophthalmol.* 2004;137(2):228–235.

59. Hougaard JL, Heijl A, Bengtsson B. Glaucoma Detection by Stratus OCT. *J Glaucoma.* 2007;16(3):302–306.

60. Shin CJ, Sung KR, Um TW, et al. Comparison of retinal nerve fibre layer thickness measurements calculated by the optic nerve head map (NHM4) and RNFL3.45 modes of spectral-domain optical

coherence tomography (RTVue-100). *Br J Ophthalmol*. 2010;94(6):763–767.

61. Cho JW, Sung KR, Hong JT, Um TW, Kang SY, Kook MS. Detection of glaucoma by spectral domain-scanning laser ophthalmoscopy/optical coherence tomography (SD-SLO/OCT) and time domain optical coherence tomography. *J Glaucoma*. 2011;20(1):15–20.

62. Wollstein G, Kagemann L, Bilonick RA, et al. Retinal nerve fibre layer and visual function loss in glaucoma: the tipping point. *Br J Ophthalmol*. 2012;96(1):47–52.

63. Ricco S, Chen M, Ishikawa H, Wollstein G, Schuman J. Correcting Motion Artifacts in Retinal Spectral Domain Optical Coherence Tomography via Image Registration. In: Yang GZ, Hawkes D, Rueckert D, Noble A, Taylor C, eds. *Medical Image Computing and Computer-Assisted Intervention – MICCAI 2009*. Lecture Notes in Computer Science. New York, NY: Springer; 2009:100–107.

64. Ortega JDL, Kakati B, Girkin CA. Artifacts on the Optic Nerve Head Analysis of the Optical Coherence Tomography in Glaucomatous and Nonglaucomatous Eyes. *J Glaucoma*. 2009;18(3):186–191.

65. Asrani S, Edghill B, Gupta Y, Meerhoff G. Optical Coherence Tomography Errors in Glaucoma. *J Glaucoma*. 2010;19(4):237–242.

66. Asrani S, Essaid L, Alder BD, Santiago-Turla C. Artifacts in spectral-domain optical coherence tomography measurements in glaucoma. *JAMA Ophthalmol*. 2014;132(4):396–402.

67. Taibbi G, Peterson GC, Syed MF, Vizzeri G. Effect of Motion Artifacts and Scan Circle Displacements on Cirrus HD-OCT Retinal Nerve Fiber Layer Thickness Measurements. *Invest Ophthalmol Vis Sci*. 2014;55(4):2251–2258.

68. Liu Y, Simavli H, Que CJ, et al. Patient Characteristics Associated With Artifacts in Spectralis Optical Coherence Tomography Imaging of the Retinal Nerve Fiber Layer in Glaucoma. *Am J Ophthalmol*. 2015;159(3):565–576.e2.

69. Ye C, Yu M, Leung CK shun. Impact of segmentation errors and retinal blood vessels on retinal nerve fibre layer measurements using spectral-domain optical coherence tomography. *Acta Ophthalmol (Copenh)*. 2016;94(3):e211–e219.

70. Thakoor KA, Koorathota SC, Hood DC, Sajda P. Robust and Interpretable Convolutional Neural Networks to Detect Glaucoma in Optical Coherence Tomography Images. *IEEE Trans Biomed Eng*. 2021;68(8):2456–2466.

71. Thakoor KA, Li X, Tsamis E, et al. Strategies to Improve Convolutional Neural Network Generalizability and Reference Standards for Glaucoma Detection From OCT Scans. *Transl Vis Sci Technol*. 2021;10(4):16.

72. Zemborain ZZ, Jarukasetphon R, Tsamis E, De Moraes CG, Ritch R, Hood DC. Optical Coherence Tomography Can Be Used to Assess Glaucomatous Optic Nerve Damage in Most Eyes With High Myopia. *J Glaucoma*. 2020;29(10):833–845.